CIRP Annals - Manufacturing Technology 75 (2026) 329–333

Contents lists available at ScienceDirect

CIRP Annals - Manufacturing Technology

journal homepage: https://www.editorialmanager.com/CIRP/default.aspx

Using single pulses in powder-blown directed energy deposition to fabricate high-aspect-ratio metal pins

Wessel W. Wits (2)[a,b,*], Shenliang Yang[c,d], Jos Vroon[a], Scholte J.L. Bremer[a]

[a] *NLR – Royal Netherlands Aerospace Centre, Marknesse, The Netherlands*
[b] *Faculty of Electrical Engineering, Mathematics and Computer Science, University of Twente, Enschede, The Netherlands*
[c] *Department of Materials Science and Engineering, University of Toronto, Toronto, Canada*
[d] *Department of Mechanical Engineering, The University of British Columbia, Vancouver, Canada*

A R T I C L E   I N F O

Article history:
Available online 6 May 2026

Keywords:
Additive manufacturing (AM)
Directed energy deposition (DED)
High-aspect-ratio metal pins

A B S T R A C T

This study investigates the fabrication of high-aspect-ratio metal pins using powder-blown directed energy deposition. Pins are deposited by consecutive laser pulses using titanium alloy Ti6Al4V as feedstock material. A physics-integrated experimental-analytical-numerical framework is developed to predict pin geometry, pin growth and thermal history during fabrication. The framework combines experimental in-situ temperature measurements, an analytical geometry model, and a finite element thermal model for melt pool lifetime predictions. Results show good agreement between model predictions and experimental observations, enabling controlled constant-diameter vertical pin growth with optimised process parameters, which is crucial for applications such as hybrid metal-composite joining and structural repair.

1. Introduction

The current state of the art in metal Additive Manufacturing (AM) combines high-precision, multi-material deposition with advanced process monitoring and simulation, enabling near-net-shape fabrication of complex, high-performance components [1]. As a distinct metal AM subclass, Directed Energy Deposition (DED) has emerged characterized by the in-situ delivery of feedstock into a melt pool generated by a focused energy source [2]. DED offers high deposition rates, multi-material capability, versatility across length scales and suitability for repair [3]. Nonetheless, the DED process is governed by highly transient multi-physical interactions among the energy source, feedstocks and molten materials, leading to melt pool instability and geometric variability [4]. As a result, existing DED studies have predominantly been applied to continuous-track-based geometries, such as thin walls and blocks [5], whereas the fabrication of discrete, high-aspect-ratio features, such as slender vertical pins, remains largely underexplored.

For application areas such as hybrid metal-composite joining and structural repair, high-aspect-ratio features are essential load-bearing elements. Pin-like structures, to improve hybrid joining technologies, have been discussed in a number of reviews [6,7]. As reported, small metal pins can significantly enhance load transfer and damage tolerance by improving interfacial shear strength while suppressing delamination [8]. To date, AM approaches using laser powder bed fusion [9] and cold-metal transfer [10] have been undertaken; however, these approaches are either difficult to implement as repair technique or fail to produce sub-millimetre-sized features [11]. As an alternative, powder-blown pulse-based DED combines geometric flexibility with repair capability, making it suitable to fabricate localised pin-like mechanical interlocking features directly on existing components without introducing additional distortion, caused by residual stresses, to the bulk component [12] and without the need for additional tooling or post-machining [13]. Moreover, DED would allow flexible control over the pin geometry, pin array density and metallurgical bonding through process parameter adjustment, facilitating tailored interlocking performance and robust load transfer in hybrid metal-composite joints.

Fabricating pins using powder-blown DED is a unique challenge. Only a single literature reference was found that showed some degree of similarity: Aladag et al. [14] describe the DED fabrication of metallic interlocking topographies; however, their goal was to create a spheroid on a cylindrical shaft, rather than a slender pin.

To realise the continuous vertical growth of a high-aspect-ratio metal pin using powder-blown, pulse-based DED, the thermal history between successive pulses needs to be fully understood. This is demonstrated in the top left inset of Fig. 1 showing initial trials with conventional process parameters leading to poor quality pins. To fill the current research gaps, in this work, a physics-integrated experimental-analytical-numerical framework is developed. The proposed framework, see Fig. 1, combines in-situ temperature measurements, an analytical geometry model, with a thermal model based on the Finite Element (FE) method. Using this framework, we (1) estimate the pin geometry growth pulse-after-pulse, (2) capture the transient temperature evolution of the pin-substrate system, and (3) quantify the melt pool lifetime for each pulse, as a metric for the pin growth rate. These results provide a quantitative guideline for enabling

* Corresponding author.
E-mail address: w.w.wits@utwente.nl (W.W. Wits).

https://doi.org/10.1016/j.cirp.2026.04.001

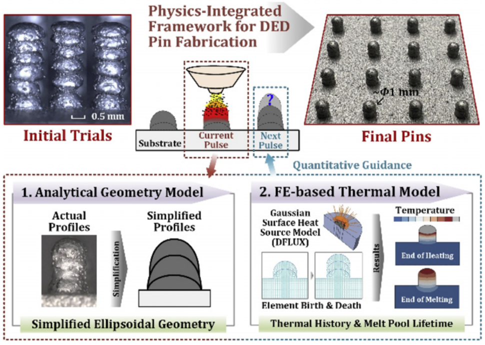

Fig. 1. Physics-integrated experimental-analytical-numerical framework for DED pin fabrication with pulse-to-pulse timing. The thermal analysis of the current pulse is used to quantitatively determine the deposition strategy for the following pulse.

controlled vertical pin growth, as demonstrated by the figure's top right inset.

2. Modelling and simulation

To model pulse-based feedstock material deposition, first an analytical model is developed to predict the deposited shape after each individual pulse based on the process parameter settings and calibrated by initial experimental observations. In a second step the resulting geometries are transferred to an FE-based model in which the thermal behaviour during fabrication is analysed.

To predict the fabricated pin geometry based on process parameters, such as laser power and pulse duration, an analytical model is developed. The model assumes that the applied laser energy is used for heating up a certain amount of material to the melting temperature during each pulse. The input laser energy $\dot{Q}_L$ is described as:

$$\dot{Q}_L = P_L t_p \eta (1 - \alpha_{loss,p}) \quad (1)$$

where, P_L is the laser power [W], t_p is the pulse time [s], η is the laser absorption factor [-] and $\alpha_{loss,p}$ is an empirical pulse-dependent loss factor [-] that accounts for thermal losses due to conduction, convection and radiation, and remelting of underlying material. The laser absorption factor defines the amount of energy that is effectively absorbed by the material. For titanium alloy Ti6Al4V this was found to be 0.45 in a precursor study [15].

The amount of material that is heated up to the melting temperature can be determined from the volumetric heat capacity:

$$\dot{Q}_{th} = m(c_p \Delta T + L) = V_m \rho (c_p (T_{melt} - T_{amb}) + L) \quad (2)$$

where, V_m represents the deposited volume [m^3], ρ is the material density [kg/m^3], c_p and L are the specific heat capacity [J/kg·K] and heat of fusion [J/kg], respectively, and T_{melt} and T_{amb} are the melting and ambient temperatures, respectively.

The deposited volume is assumed to have a hemispheroidal shape flattened along the deposition direction (z-axis), following:

$$V_m = \frac{1}{2} \cdot \frac{4}{3} \pi r^3 f_{ecc,p} \quad (3)$$

where, r is the sphere radius [m] and $f_{ecc,p}$ is a pulse-dependent eccentricity factor [-] that flattens the sphere to a spheroid, as illustrated in Fig. 2(a). Due to remelting of the underlying material, the hemispheroidal volume is redistributed such that (molten) material

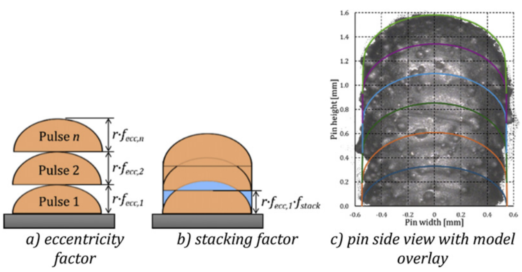

Fig. 2. Build-up of the analytical model: (a) flattening and (b) stacking of consecutive pulses, and (c) results of a six-pulse calibrated model.

from the top of the underlying spheroid is relocated to the circumference forming a high-aspect-ratio pin. Hereto, an empirical stacking factor f_{stack} of 0.6 is defined that lowers the pulse stacking height, as illustrated in Fig. 2(b).

Both pulse-dependent factors, listed in Table 1, are determined empirically based on an initial deposition trial in which six pins are fabricated next to each other with an incrementing number of pulses from 1 to 6. For the first two pulses, thermal losses are higher due to the presence of the substrate representing a large thermal mass that quickly conducts heat away. From Pulse 3 onwards a steady-state situation is reached in which the deposited pin itself determines the dominant loss factor. Similarly, for Pulse 1 the eccentricity factor is governed by the initial material deposition on the flat substrate, while for Pulse 2 onwards the factor is determined by the spheroid's top of the previous pulse.

Table 1
Pulse-dependent thermal loss factor and eccentricity factor.

Pulse no.	1	2	3	4	5	6
$\alpha_{loss,p}$	0.89	0.85	0.79	0.79	0.79	0.79
$f_{ecc,p}$	0.60	0.75	0.75	0.75	0.75	0.75

Fig. 2(c) illustrates the result of the analytical model following Eqs. (1)–(3). Each pulse is represented by a hemispheroidal shape stacked on top of each other. In the figure, the result is overlaid on a trial pin fabricated by six consecutive pulses. The resulting stacked hemispheroidal shapes are transferred to the FE thermal analysis to model the pulse-wise material deposition.

The commercial FE solver ABAQUS is employed to simulate the thermal responses of the pin-substrate system during the pulse-by-pulse DED process. Fig. 3 illustrates the initial geometry, pulse-based element meshing strategy and thermal boundary conditions of the developed FE model.

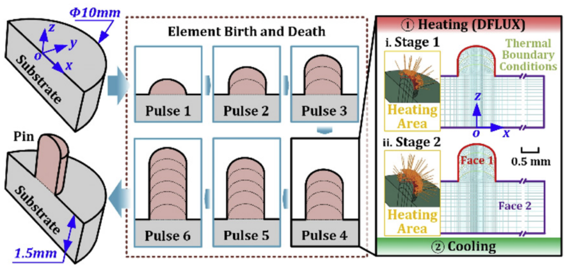

Fig. 3. Overview of the FE-based modelling strategy for predicting the temperature evolution during pulse-based DED fabrication of high-aspect-ratio metal pins.

At the start of the simulation, all elements associated with the pin are deactivated. The pin is then grown vertically following a pulse-by-pulse manner by sequentially activating the corresponding elements according to the afore-predicted hemispheroidal shapes and pre-defined deposition time. Each pulse involves a two-step thermal analysis: heating and cooling. During heating, the top surface of the substrate for Pulse 1 or the previously deposited material for the following pulses is heated over an initial 0.002 s (Stage 1). After that, elements associated with the current pulse are activated and the heating region shifts to the top surface of the newly added material with the convective and radiative heat transfer boundary conditions updated accordingly (Stage 2).

Predicting the temperature of the pin-substrate system is based on resolving the 3D heat transfer partial differential equation, also known as the heat equation. Linear heat transfer elements (DC3D8) are employed. The mesh size used for the pin is set to 50 μm, while the mesh size becomes coarser from the pin to the substrate's bottom and side surfaces, in order to enhance the computational efficiency. A total of 35,598 DC3D8 elements are involved in the thermal analysis capturing half of the pin-substrate system under a circular symmetry assumption to reduce computational cost. Note that, during each pulse, only activated elements are involved in the transient thermal analysis at each time increment, whereas inactivated elements are excluded from the temperature update. Temperatures over time and space are computed based on temperature-dependent material properties, including ρ, c_p, and k. Values are taken from [16]. The Gaussian surface heat source model is used to represent the energy input of the laser source to the system in the pulse-based DED process, which is formulated as:

$$\dot{q} = \frac{P_L \eta}{2\pi r_0^2} exp\left[-\frac{(x-x_0)^2 + (y-y_0)^2}{2r_0^2}\right] \tag{4}$$

where, (x_0, y_0) refers to the centre of the heat source model and r_0 is defined as the radius of the heat source spot size [m]. For each subsequent pulse, the application of the heat source model to the corresponding heating region per time increment is implemented through the ABAQUS user-subroutine DFLUX.

Cooling, due to convection and radiation, are captured by Newton's law of cooling and Stefan-Boltzmann law of radiation:

$$\dot{q}_c = h_c(T - T_{amb}) \tag{5}$$

$$\dot{q}_r = \sigma\varepsilon(T^4 - T_{amb}^4) \tag{6}$$

where, q_c and q_r are the convective and radiative heat fluxes across the exposed surfaces of the pin-substrate system to the environment, respectively. h_c is the heat convection coefficient [W/m^2·K], which is defined as temperature-dependent. Values are taken from [16] suggesting that the deposit that is in direct contact with the shielding gas flow results in a higher forced convection heat loss from the pin surface (Face 1 in Fig. 3) compared to the substrate surface (Face 2). ε refers to the material's emissivity [-] with all the exposed surfaces sharing the same value of 0.425. σ represents the Stefan-Boltzmann constant, and T_{amb} is the ambient temperature in the DED build chamber, which is set to 300 K.

3. Experimental approach

A BeAM Modulo 400, equipped with an IPG YLS-2000 fibre laser with a 0.33 mm laser beam waist radius and Medicoat Flowmotion powder feeders, is employed to fabricate the pins. The Modulo 400 contains an inert build chamber filled with argon, in which the pins are deposited in a pulse-wise manner. The deposition process is monitored by two camera systems, a conventional daylight camera and an InfraRed (IR) thermal camera. Post-process optical microscopy using a Keyence VHX-1000 digital light microscope is used to determine the width and height of each pin.

For each trial, six pins are deposited next to each other. Pin 1 is formed by a single pulse following a stepwise increase in the number of pulses to Pin 6 consisting of 6 consecutive pulses, see top left inset of Fig. 4. For each pulse, the laser is turned on for the minimum pulse duration determined by the DED system. The first pulse is always deposited with both the laser and powder focal planes at the substrate surface. Follow-up pulses commence at approximately 0.7 s intervals, in which time the deposition head is moved upwards by 0.34 mm as well. During pin deposition a continuous mass flow of 1 g/min carried by an argon carrier gas flow of 3 L/min is attained. The powder flow is shaped by a central argon gas flow of 3 L/min and a secondary gas flow of 6 L/min. Aerospace qualified titanium alloy Ti6Al4V is used as powder feedstock and substrate material.

The thermal history of Pin 6 is captured by a thermocouple positioned at the bottom of the substrate aligned with the pin's central axis, as well as by the thermal camera. The thermocouple is connected to a Eurotherm 6100A recorder with a 8 Hz sample rate. The thermal camera is a FLIR A70 which is positioned inside the build chamber observing the pin fabrication from a side view. The deposition is captured with a framerate of 30 Hz and a resolution of 640 × 480 pixels. Fig. 4 shows the complete experimental setup including the viewing angle of the thermal camera, a snapshot of the thermal camera recording during Pulse 1, as well as two sets of fabricated pins from a 1-pulse pin to a 6-pulse pin.

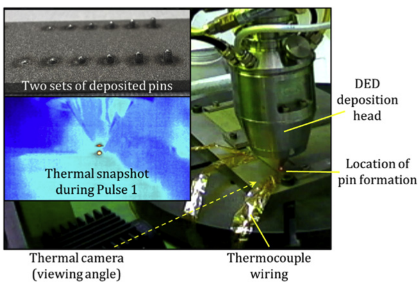

Fig. 4. Overview of the experimental setup; insets show two sets of fabricated pins and a snapshot of the thermal camera recording.

4. Results and discussion

After extensive trial-and-error experimentation and continuous microscopic observations, the process parameters listed in Table 2 were found to result in pins with a consistent small diameter and a uniform pulse-to-pulse connection. As the initial two pulses dissipate more heat to the substrate compared to subsequent pulses, a higher initial laser power is required to realise stable pin growth. For further model validation, the fabrication of Pins 1–6 is repeated four times following the process settings of Table 2.

Table 2
Optimised DED process parameter settings.

	Laser power [W]	Pulse time [s]	Delay time [s]
Pulse 1	291	0.066	0.632
Pulse 2	234	0.068	0.638
Pulse 3	177	0.068	0.634
Pulse 4	177	0.068	0.638
Pulse 5	177	0.068	0.632
Pulse 6	177	0.066	-

The top insets of Fig. 5 depict the fabrication results of one set of pins. The sequence shows the development of a high-aspect-ratio pin, stable pin growth per pulse, as well as a consistent pin diameter. The measured pin dimensions, i.e., width and height, determined after each pulse of the four sets, are indicated in the graph by the grey lines. The black line indicates the results of the analytical model. The graph shows that a good correlation between the model and experiment is obtained. In general, the pin geometry after each pulse can be predicted with 5% accuracy. Also, the individual experiments show relatively low variability indicating a stable process window.

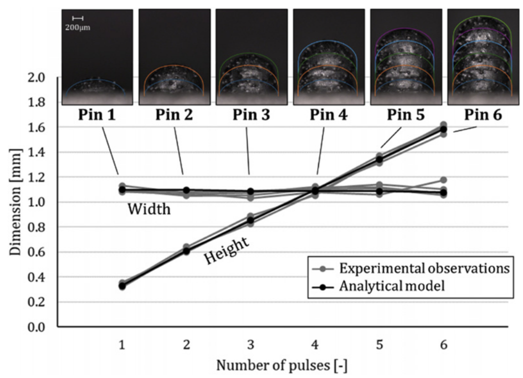

Fig. 5. Pin dimensions following six consecutive DED pulses; top insets depict the individual pins including an overlay of the analytical model.

Fig. 5 shows that the pin diameter does not change due to the consecutive pulses. Compared to the results of the initial trials as depicted in the Fig. 1 top left inset, the current process parameters, in which Pulses 1 and 2 are adjusted compared to Pulses 3 to 6 to account for the thermal influence of the substrate, are better optimised. In this case, the pin diameter is around 1.1 mm; however, by adjusting e.g., the powder mass flow rate this could be further enhanced. The pin growth rate per pulse is also relatively constant with an average growth of 0.25 mm per pulse except for Pulse 1 in which the initial hemispheroid, without material redistribution, has an average height of 0.33 mm.

The measured temperature profiles of two independently fabricated 6-pulse pins are compared to the simulation results from the developed thermal model at two selected locations. The temperature at Focal Point 1 (FP1) measured by the thermocouple attached to the substrate's bottom surface, is shown in Fig. 6(a). The measured temperatures follow a gradual, piecewise-smooth increase at each pulse-induced inflection point. The measured pulse-to-pulse temperature increments at FP1 gradually decrease during fabrication, due to the increasing heat conduction length between the measurement point and the heating location as the pin grows, as well as the enlarged convective and radiative heat losses due to the progressively larger pin surfaces.

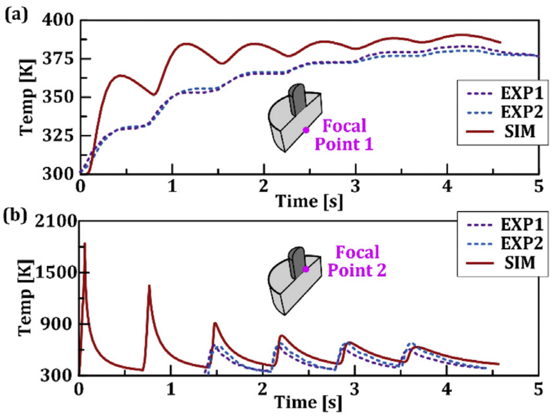

Fig. 6. Comparison of the simulated temperature profiles with the measured temperatures at (a) Focal point 1 and (b) Focal point 2.

The gradually increasing temperature at FP1 is also captured by the model; however, the predicted temperatures are consistently higher than the measurements. This discrepancy can be attributed to a higher effective heat input to the modelled pin-substrate system, due to the neglected heat losses related to the catchment efficiency; i.e., not all heated powder particles are caught by the melt pool. Due to the continuous shielding gas flow, a small fraction of the heated powder particles is dispersed, thereby carrying thermal energy away from the pin-substrate system. As a result, more energy is brought into the pin-substrate system compared to the experiment, resulting in an overestimation of the predicted thermal history at FP1. The overestimation decreases as the pin grows due to higher heat dissipation at elevated temperatures.

Focal Point 2 (FP2) tracks the temperature at the base of the pin, as shown in Fig. 6(b). Here, the measured temperature profiles are captured by the IR camera with the focal point at the pin circumference just above the pin-substrate interface. During the first two pulses no solid material is presented here and the IR camera is observing the melt pool directly leading to saturated images. The first two simulated peak temperatures also indicate that melting temperatures are reached here. From Pulse 3 onwards, the measured temperature profiles are reliably captured and shown in the figure. As the pin continues to grow after Pulse 3, the measured and predicted temperature profiles compare well, demonstrating that the developed FE model is capable of capturing the transient temperature evolution of the pin-substrate system based on the elemental shapes predicted by the analytical model.

From the thermal simulation, the melt pool lifetime, referring to the time duration between the start of laser heating and the end of melting, can be determined. This is illustrated in Fig. 7. The variability in melt pool lifetime is determined from the variation in actual fabricated pin geometries (Fig. 5). During the melt pool lifetime, the pin is capable of capturing mass flow and hence grows. The figure shows a relatively stable melt pool lifetime, in particular after the second pulse, which corresponds well with the constant pin growth rate as observed in Fig. 5.

Based on the measured pulse-to-pulse geometries of Fig. 5, the average mass increment per pulse can be determined. Similarly, Eq. (2) of the analytical model can also be used to predict the mass increment per pulse. Finally, from the powder mass flow rate, the particle-accepting melt pool lifetime (Fig. 7) and the catchment efficiency, the mass increment per pulse can be estimated as well. These results are shown in Fig. 8, in which the shaded area encompasses the prediction

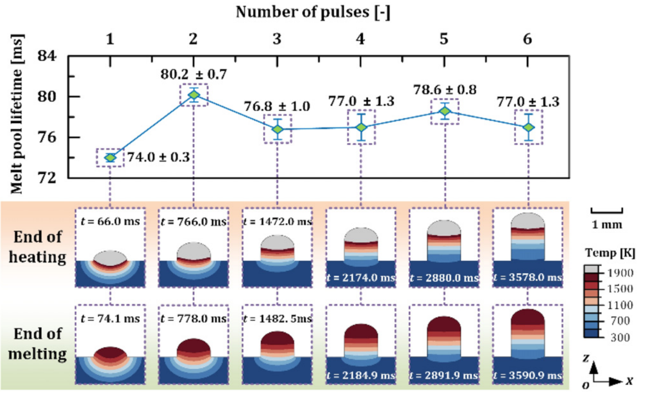

Fig. 7. The evolution of melt pool lifetime pulse by pulse and the temperature distribution in the pin-substrate system during DED.

between 80% to 100% catchment efficiency. The figure shows that relatively good agreement between the three analysis methods is achieved. As afore, a small powder fraction is likely dispersed leading to a best fit at 84% powder catchment efficiency. Of particular interest is the observation that the melt pool lifetime can be correlated to the pin mass growth rate. This may lead to further guidance in tuning DED process parameters for particular pin growth requirements.

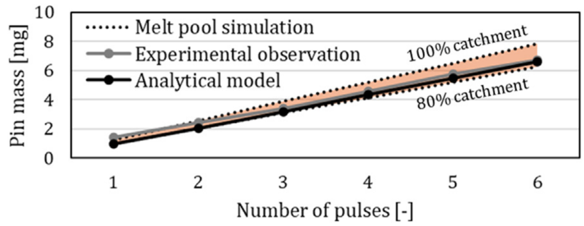

Fig. 8. Three analysis methods to capture the mass evolution per pulse.

5. Conclusions

This study demonstrates the development of a physics-integrated experimental-analytical-numerical framework for predicting the thermal history and growth of high-aspect-ratio metal pins fabricated using powder-blown pulse-based DED. An analytical model that predicts pulse-wise geometric pin growth is used as input for an FE thermal model. The results show good agreement between experimental observations and model predictions, substantiating the validity of this novel approach. High-aspect-ratio metal pins have been fabricated realising a consistent pin growth rate using an optimised pulse-based process parameter set. Future work will include further pin growth strategies by optimising mass flow rate, laser power, and pulse and waiting times, and analysing effects thereof by the thermal model.

Declaration of competing interest

The authors declare that they have no known competing financial interests or personal relationships that could have appeared to influence the work reported in this paper.

CRediT authorship contribution statement

Wessel W. Wits: Writing – review & editing, Writing – original draft, Visualization, Validation, Supervision, Project administration, Methodology, Funding acquisition, Formal analysis, Conceptualization. **Shenliang Yang:** Writing – original draft, Visualization, Validation, Methodology, Investigation, Formal analysis, Data curation, Conceptualization. **Jos Vroon:** Writing – original draft, Visualization, Methodology, Investigation. **Scholte J.L. Bremer:** Writing – original draft, Investigation.

Acknowledgements

This research is conducted within the research and innovation programme Luchtvaart in Transitie, which is co-funded by the Netherlands National Growth Fund.

References

[1] Chen Y, et al. (2020) A Review on Metallic Alloys Fabrication Using Elemental Powder Blends by Laser Powder Directed Energy Deposition Process. *Materials* 13 (16):3562. https://doi.org/10.3390/ma13163562.

[2] DebRoy T, et al. (2018) Additive Manufacturing of Metallic Components – Process, Structure and Properties. *Progress in Materials Science* 92:112–224. https://doi.org/10.1016/j.pmatsci.2017.10.001.

[3] Liu M, Kumar A, Bukkapatnam S, Kuttolamadom M (2021) A Review of the Anomalies in Directed Energy Deposition (DED) Processes & Potential Solutions - Part Quality & Defects. *Procedia Manufacturing* 53:507–518. https://doi.org/10.1016/j.promfg.2021.06.093.

[4] Clare AT, et al. (2025) Metal Multi-Material Additive Manufacturing: Overcoming Barriers to Implementation. *CIRP Annals* 74(2):869–893. https://doi.org/10.1016/j.cirp.2025.05.004.

[5] Li Z, et al. (2022) High Deposition Rate Powder- and Wire-Based Laser Directed Energy Deposition of Metallic Materials: A Review. *International Journal of Machine Tools and Manufacture* 181:103942. https://doi.org/10.1016/j.ijmachtools.2022.103942.

[6] Lambiase F, et al. (2021) A State-of-the-Art Review on Advanced Joining Processes for Metal-Composite and Metal-Polymer Hybrid Structures. *Materials* 14(8):1890. https://doi.org/10.3390/ma14081890.

[7] Galińska A, Galiński C, Galińska A, Galiński C (2020) Mechanical Joining of Fibre Reinforced Polymer Composites to Metals—A Review. Part II: Riveting, Clinching, Non-Adhesive Form-Locked Joints, Pin and Loop Joining. *Polymers* 12(8):1681. https://doi.org/10.3390/polym12081681.

[8] Bagnato T, et al. (2023) Superior Interfacial Toughening of Hybrid Metal-Composite Structural Joints Using 3D Printed Pins. *Composites Part A: Applied Science and Manufacturing* 168:107479. https://doi.org/10.1016/j.compositesa.2023.107479.

[9] Parkes PN, Butler R, Meyer J, de Oliveira A (2014) Static Strength of Metal-Composite Joints With Penetrative Reinforcement. *Composite Structures* 118:250–256. https://doi.org/10.1016/j.compstruct.2014.07.019.

[10] Ucsnik S, Scheerer M, Zaremba S, Pahr DH (2010) Experimental Investigation of a Novel Hybrid Metal–Composite Joining Technology. *Composites Part A: Applied Science and Manufacturing* 41(3):369–374. https://doi.org/10.1016/j.compositesa.2009.11.003.

[11] Wei C, Zhang Z, Cheng D, Sun Z, Zhu M, Li L (2021) An Overview of Laser-Based Multiple Metallic Material Additive Manufacturing: From Macro- To Micro-Scales. *International Journal of Extrememe Manufacturing* 3(1):012003. https://doi.org/10.1088/2631-7990/abce04.

[12] Bendeich P, et al. (2006) Residual Stress Measurements in Laser Clad Repaired Low Pressure Turbine Blades for the Power Industry. *Materials Science and Engineering: A* 437(1):70–74. https://doi.org/10.1016/j.msea.2006.04.065.

[13] Wilson JM, Piya C, Shin YC, Zhao F, Ramani K (2014) Remanufacturing of Turbine Blades by Laser Direct Deposition With Its Energy and Environmental Impact Analysis. *Journal of Cleaner Production* 80:170–178. https://doi.org/10.1016/j.jclepro.2014.05.084.

[14] Aladag M, Zglobicka I, Marquadt F, Stepien L, Lopez E, Kurzydlowski KJ (2025) Failure Analysis Approach to Designing Interlocking of Polymer Thick Coats on Metallic Substrates. *Journal of Materials Research and Technology* 39:5358–5366. https://doi.org/10.1016/j.jmrt.2025.10.049.

[15] Vroon J, Van der Eems A, Van der Brink W (2023) Thermal and Mechanical Calibration of Multi-Material DED AM Process Simulations on Part-Scale. *IVth International Conference on Simulation for Additive Manufacturing (Sim-AM 2023)*, 12. https://doi.org/10.23967/c.simam.2023.003.

[16] Lu X, et al. (2018) Finite Element Analysis and Experimental Validation of the Thermomechanical Behavior in Laser Solid Forming of Ti-6Al-4V. *Additive Manufacturing* 21:30–40. https://doi.org/10.1016/j.addma.2018.02.003.